

Substrate Grain-Dependent Chemistry of Carburized Planar Anodic TiO₂ on Polycrystalline Ti

Celine Rüdiger,^{*,†,‡} Marco Favaro,^{‡,∇} Carlos Valero-Vidal,^{§,○} Laura Calvillo,[‡] Nathalie Bozzolo,^{||} Suzanne Jacomet,^{||} Jennifer Hein,^{⊥,◆} Luca Gregoratti,[#] Stefano Agnoli,^{‡,Ⓜ} Gaetano Granozzi,^{‡,Ⓜ} and Julia Kunze-Liebhäuser^{*,§}

[†]Physik-Department, Technische Universität München, James-Franck-Str. 1, 85748 Garching, Germany

[‡]Dipartimento di Scienze Chimiche, Università di Padova, Via Marzolo 1, 35131 Padova, Italy

[§]Institut für Physikalische Chemie, Leopold-Franzens-Universität Innsbruck, Innrain 52c, 6020 Innsbruck, Austria

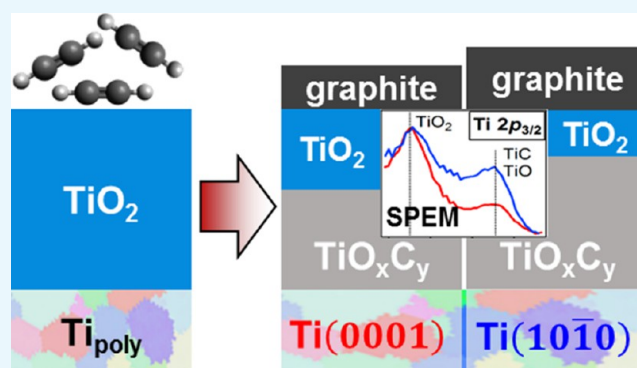
^{||}CEMEF - Centre de Mise en Forme des Matériaux, MINES ParisTech, PSL Research University, CNRS UMR 7635, CS 10207 Rue Claude Daunesse, 06904 Sophia Antipolis Cedex, France

[⊥]Lehrstuhl für Technische Chemie II, Technische Universität München, Lichtenbergstr. 4, 85748 Garching, Germany

[#]Elettra – Sincrotrone Trieste SCpA, SS14-Km163.5 in Area Science Park, 34149 Trieste, Italy

Supporting Information

ABSTRACT: Mixtures or composites of titania and carbon have gained considerable research interest as innovative catalyst supports for low- and intermediate-temperature proton-exchange membrane fuel cells. For applications in electrocatalysis, variations in the local physicochemical properties of the employed materials can have significant effects on their behavior as catalyst supports. To assess microscopic heterogeneities in composition, structure, and morphology, a microscopic multitechnique approach is required. In this work, compact anodic TiO₂ films on planar polycrystalline Ti substrates are converted into carbon/titania composites or multiphase titanium oxycarbides through carbothermal treatment in an acetylene/argon atmosphere in a flow reactor. The local chemical composition, structure, and morphology of the converted films are studied with scanning photoelectron microscopy, micro-Raman spectroscopy, and scanning electron microscopy and are related with the crystallographic orientations of the Ti substrate grains by means of electron backscatter diffraction. Different annealing temperatures, ranging from 550 to 850 °C, are found to yield different substrate grain-dependent chemical compositions, structures, and morphologies. The present study reveals individual time scales for the carbothermal conversion and subsequent surface re-oxidation on substrate grains of a given orientation. Furthermore, it demonstrates the power of a microscopic multitechnique approach for studying polycrystalline heterogeneous materials for electrocatalytic applications.



1. INTRODUCTION

In catalysis and electrocatalysis, a detailed understanding of the local physicochemical properties of the active materials is of utmost importance to develop optimized functional materials. Many fundamental investigations on catalytic materials are based on the study of single crystalline substrates because their well-defined surfaces facilitate the relation of materials properties to observed processes, such as pathways of catalytic reactions that are promoted on differently oriented crystalline surfaces.^{1–3} However, real catalyst materials require a high surface area and are synthesized in the form of supported nanoparticles or high-surface-area powders, which in most cases bring about nanoscopically or microscopically heterogeneous physicochemical properties. In view of the important role of the






support, which needs to stabilize the catalyst nanoparticles, to ensure electrical conductivity or which under certain conditions can positively influence the overall catalytic performance, it is necessary to devote sufficient research efforts to the investigation of innovative support materials on a microscopic basis. A model system that constitutes a compromise between real high-surface-area powders and a well-defined single crystalline surface with assessable properties is provided by a polycrystalline planar substrate. With the emergence of experimental methods that combine microscopy with comple-

Received: December 6, 2016

Accepted: January 27, 2017

Published: February 21, 2017

Table 1. Ranges of Ti Substrate Orientations and Representative Projected Hexagonal Cells

tilt angle Φ of Ti	$0^\circ \leq \Phi \leq 15^\circ$	$15^\circ \leq \Phi \leq 40^\circ$	$40^\circ \leq \Phi \leq 50^\circ$	$50^\circ \leq \Phi \leq 90^\circ$ ($\sim\text{Ti}\{hki0\}$)
azimuthal φ_2 orientation of Ti		$0^\circ \leq \varphi_2 \leq 30^\circ$		$0^\circ \leq \varphi_2 \leq 15^\circ$ $15^\circ \leq \varphi_2 \leq 30^\circ$
Ti(hki)	$\sim\text{Ti}(0001)$			$\sim\text{Ti}\{10\bar{1}0\}$ $\sim\text{Ti}\{2\bar{1}\bar{1}0\}$
color representation	red	orange	purple	blue green
label	A	B	C	D E
representative hexagonal cell				 

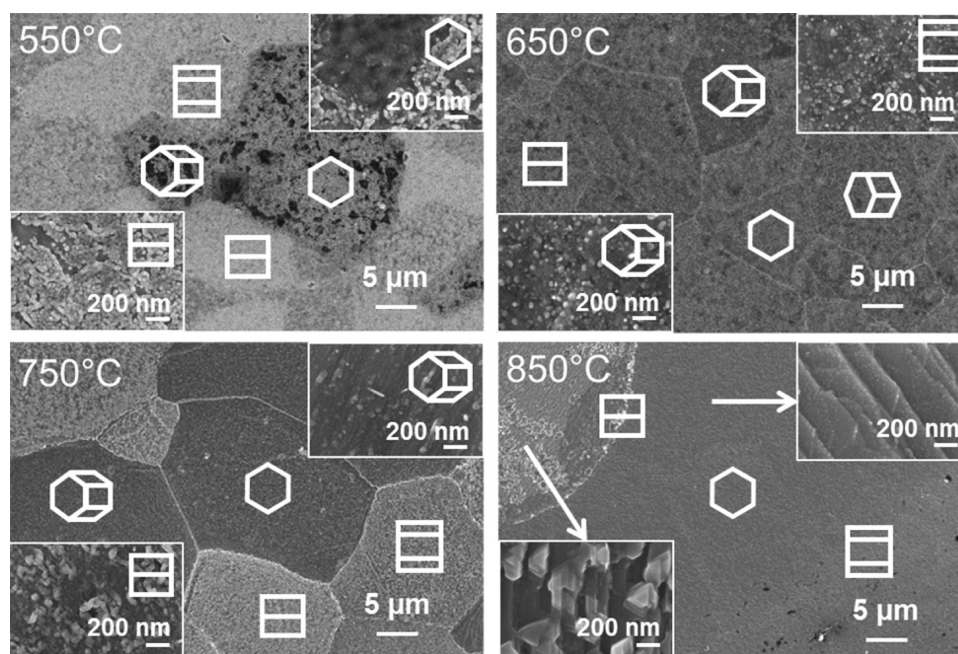


Figure 1. Scanning electron micrographs of TiOC. High-magnification insets: areas on differently oriented substrate grains (TiOC_{550} , TiOC_{650} , TiOC_{750}) or areas with different TiOC morphologies (TiOC_{850}). Projected hexagonal cells: approximate crystallographic orientation of the Ti substrate grains.

mentary analysis methods, such as photoelectron or vibrational spectroscopy, diffractometry, or electrochemistry, the investigation of planar polycrystalline materials has opened up new perspectives in materials research.^{4–7}

Hybrid or composite materials of titania and carbon (Ti–O–C) have gained remarkable interest in the search for suitable catalyst support materials for proton-exchange membrane fuel cells, as they may provide a higher corrosion resistance than that of commonly used carbon-based supports in combination with a high electrical conductivity^{8–10} and may enhance the overall catalytic activity.^{11–13} Planar model systems consisting of thermally carburized compact anodic titania films on a polycrystalline titanium substrate (Ti_{poly}) provide a flexible model system to study the relationship between the physicochemical properties of Ti–O–C materials, which can be tailored via the synthesis conditions, and their electrochemical and electrocatalytic performances.^{14–16} In particular, different annealing temperatures during the carbothermal treatment of anodic TiO_2 yield significantly different average physicochemical properties of the obtained Ti–O–C films,¹⁴ which in turn strongly affect the catalytic properties of Ti–O–C-supported Pt nanoparticles (Pt/Ti–O–C) toward the electrochemical oxidation of ethanol in an acidic electrolyte.¹⁵ Interestingly, a clear influence of the Ti substrate grains on the

local (electro)chemical stability of Pt/Ti–O–C on Ti_{poly} was observed,¹⁵ which demonstrates the necessity for the use of microscopic analysis tools to gain a deep understanding of the local property–performance relationships on such model systems. In a previous publication, we have investigated the effect of titanium substrate grain orientations on the crystallization of compact anodic TiO_2 and on the reactive decomposition of acetylene during carbothermal treatment with acetylene at a relatively low annealing temperature. A substrate grain-dependent chemical composition and structure of the obtained C/TiO₂ composite material has been observed in this study.⁷ The effect of annealing temperature on the final average composition of Ti–O–C films, prepared at relatively high temperatures, has been explained with a thermodynamic model, where diffusion of carbon and oxygen in the compact anodic TiO_2 has been taken into account.¹⁴ A common consideration of both substrate grain orientation and annealing temperature is still missing. However, it is necessary to gain a deeper understanding and control of the synthesis of such Ti–O–C systems.

Therefore, in the present study, the effect of annealing temperature on the substrate grain-dependent physicochemical properties of carburized planar anodic TiO_2 films on Ti_{poly} is investigated using both microscopic and spectroscopic

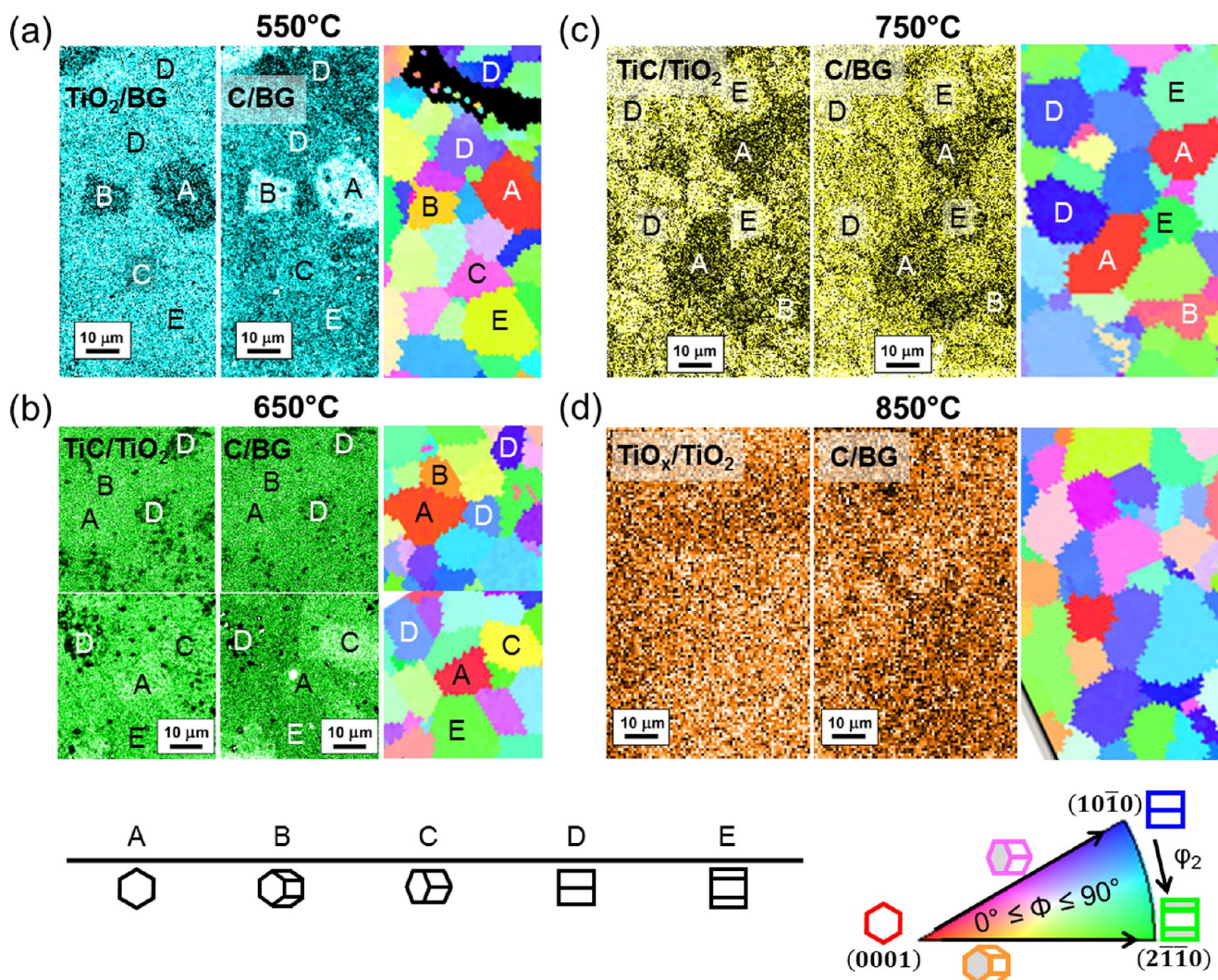


Figure 2. Chemical maps from Ti $2p_{3/2}$ (always left) and C $1s$ (always center) photoelectron micrographs of TiOC, and EBSD maps (always right) of the corresponding Ti substrate. (a) TiOC₅₅₀, (b) TiOC₆₅₀, (c) TiOC₇₅₀, and (d) TiOC₈₅₀. To facilitate discrimination between the different TiOCs, the chemical maps are differently colored. Table: approximate orientation of the labeled grains. Standard triangle: color-orientation code of the EBSD maps.

techniques. Ti–O–C films are synthesized via carbothermal treatment with acetylene at four different annealing temperatures, that is, 550, 650, 750, and 850 °C. Scanning electron microscopy (SEM), scanning photoelectron microscopy (SPEM), and micro-Raman spectroscopy results of the carburized films are correlated with the crystallographic orientation of the substrate grains, which is assessed through electron backscatter diffraction (EBSD).

2. RESULTS

EBSD was used to generate crystalline orientation maps of the Ti_{poly} substrates, which will be represented as surface-normal projected inverse pole figure orientation maps in the following. From these maps, the orientations of the hexagonal lattice of Ti with respect to the substrate surface, defined by the three Euler angles, are extracted for individual grains.

To define the crystallographic plane parallel to the sample surface, only the two Euler angles, Φ and φ_2 , need to be considered.¹⁷ Angle Φ describes the tilt of the c -axis of the hexagonal unit cell with respect to the substrate surface, and φ_2 describes the azimuthal rotation of the hexagonal unit cell about

its c -axis with respect to a reference orientation with $\varphi_2 = 0^\circ$. Because of the hexagonal symmetry, the values of the orientation angles can be restricted to $0^\circ \leq \Phi \leq 90^\circ$ and $0^\circ \leq \varphi_2 \leq 30^\circ$. According to our previous work, it is sufficient to take into account four ranges of tilt angles, Φ , to gain insight into the physicochemical properties of thermally treated planar anodic TiO₂ films.⁷ In addition, we subdivide the orientations with $\Phi > 50^\circ$ into $0^\circ \leq \varphi_2 \leq 15^\circ$ and $15^\circ \leq \varphi_2 \leq 30^\circ$. Table 1 lists the five groups of Ti substrate orientations that are considered in the present study and shows the surface-projected hexagonal cells that are used for labeling.

Figure 1 shows scanning electron micrographs of TiOC, synthesized at different temperatures. After the thermal treatments at temperatures of up to 750 °C, the grain boundaries of the Ti substrate are still visible through the TiOC. The morphology of TiOC₅₅₀ and TiOC₇₅₀ is clearly affected by the crystallographic orientation of the underlying Ti substrate grains. In particular, substrate grains with tilt angles $0^\circ \leq \Phi \leq 40^\circ$ can be easily distinguished from substrate grains with tilt angles $\Phi \geq 50^\circ$, due to apparent differences in the morphologies of the TiOC overlayers. TiOC₆₅₀ is characterized

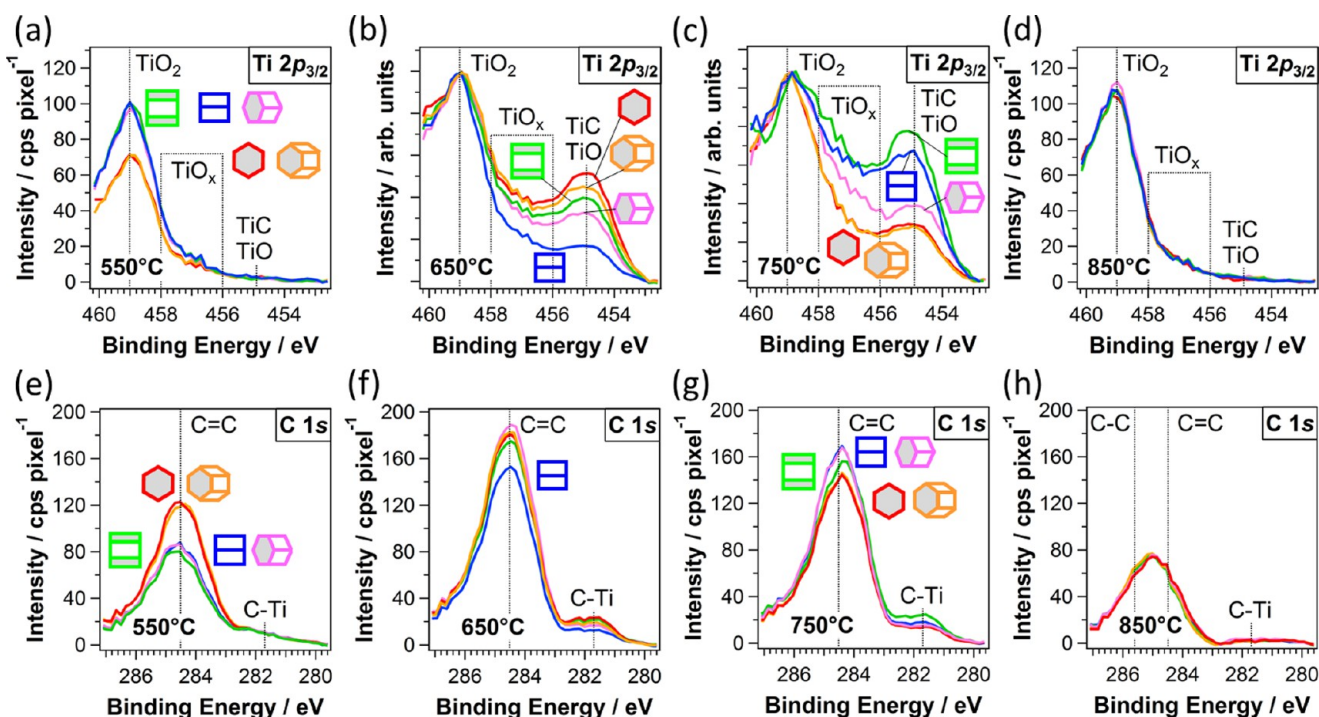


Figure 3. Spectra from Ti $2p_{3/2}$ (top) and C $1s$ (bottom) core-level maps of TiOC, acquired on top of substrate grains with five different orientations, as indicated by the hexagonal cells using the color-orientation code. (a, e) TiOC₅₅₀, (b, f) TiOC₆₅₀, (c, g) TiOC₇₅₀, and (d, h) TiOC₈₅₀. The spectra in (b, c) are scaled to the TiO₂ component height.

by a granular morphology with no pronounced substrate grain dependency; only the grain boundaries can be recognized. After carbothermal treatment at 850 °C, the initial grain boundaries of the substrate disappeared and extended areas of uniform morphology formed. No interdependence between morphology and the original substrate grain orientation is visible due to significant substrate grain growth at this temperature.¹⁸

The comparison between the morphologies of TiOC₇₅₀ and TiOC₈₅₀ suggests that the surface undergoes an ordering at high annealing temperatures. The high-resolution micrographs (insets) of TiOC₈₅₀ show ordered morphologies, such as triangular shapes (left bottom) or stepped terraces (right top). The phase change of the Ti substrate from α -Ti (hcp structure) to β -Ti (bcc structure) does not happen below 882 °C and can therefore not be responsible for this ordering.¹⁹

Figure 2 depicts chemical maps of the Ti $2p_{3/2}$ and C $1s$ core-level electrons extracted from SPEM of TiOC and the corresponding EBSD maps of the Ti substrate. Apparently, the surface chemistry of TiOC₅₅₀ and TiOC₇₅₀ is affected by the orientation of the substrate grains: TiOC films on type A and B grains ($0^\circ \leq \Phi \leq 40^\circ$, $\sim\text{Ti}(0001)$) show a clearly different average brightness in the chemical maps than that of films on type D and E grains ($50^\circ \leq \Phi \leq 90^\circ$, $\sim\text{Ti}\{hkil\}$). In the case of TiOC₇₅₀, several grain boundaries can be identified. On the other hand, the surface of TiOC₈₅₀ has a relatively homogeneous composition that is independent of the substrate grains in the mapped area. The chemical maps of TiOC₆₅₀ show several areas with dark spots and less pronounced grain boundaries.

For each type of substrate grain, X-ray photoelectron (XP) spectra of the Ti $2p_{3/2}$ and C $1s$ core levels are extracted from the photoelectron maps and plotted in Figure 3. Each spectrum is obtained from a rectangular area on a substrate grain and represents the average surface composition of TiOC on that

grain. An alternative representation of the XP spectra is given in Figures S1 and S2 in the Supporting Information (SI). The Ti $2p_{3/2}$ signals show that all TiOCs contain TiO₂ (459 eV)⁵ and that TiOC₆₅₀ and TiOC₇₅₀ additionally contain a considerable fraction of TiC and/or TiO species (454.9 eV)^{5,20} and some TiO_x sub-oxides (456–458 eV, $1 < x < 2$)^{5,14} at the surface.

In the case of TiOC₅₅₀, TiOC₆₅₀, and TiOC₇₅₀, the pronounced peak in the C $1s$ spectra, centered at 284.5 eV, is attributed to an sp^2 -hybridized (graphitic) carbon (C=C) (Figure 3e–g).^{5,21} The C $1s$ peak found for TiOC₈₅₀ (Figure 3h) is shifted toward the binding energy of an sp^3 -hybridized (diamond-like) carbon (C–C at 285.6 eV),^{5,21} indicating the presence of amorphous carbon on the surface.²² It can be seen that only TiOC₆₅₀ and TiOC₇₅₀ contain a notable amount of carbidic carbon (281.7 eV) within a film depth of ~ 1.4 – 2.3 nm (calculated for TiO₂ and C=C), which is analyzed with SPEM.²¹

Analysis of the XP spectra reveals that carbothermal treatment at 550 °C mainly produces graphitic carbon on top of TiO₂. A significant reduction in the anodic TiO₂ film is obtained through carbothermal treatments at 650 and 750 °C, generating TiC (TiO) and TiO_x species, and the resultant TiOC is covered by a relatively high amount of graphitic carbon. The surface of TiOC₈₅₀ consists of TiO₂ covered by amorphous carbon.

Both chemical maps (Figure 2) and XP spectra (Figure 3) show that the conversion from TiO₂ to TiC (TiO) and TiO_x depends both on the annealing temperature and substrate texture. On TiOC₅₅₀ (Figures 2a and 3a,e), the relative amount of graphitic carbon is significantly enhanced and the fraction of TiO₂ is small on top of substrate grains of types A and B ($\sim\text{Ti}(0001)$), with $0^\circ \leq \Phi \leq 40^\circ$. A detailed investigation on the effect of substrate grains on the chemical surface composition of TiOC₅₅₀ has been published elsewhere.⁷ The

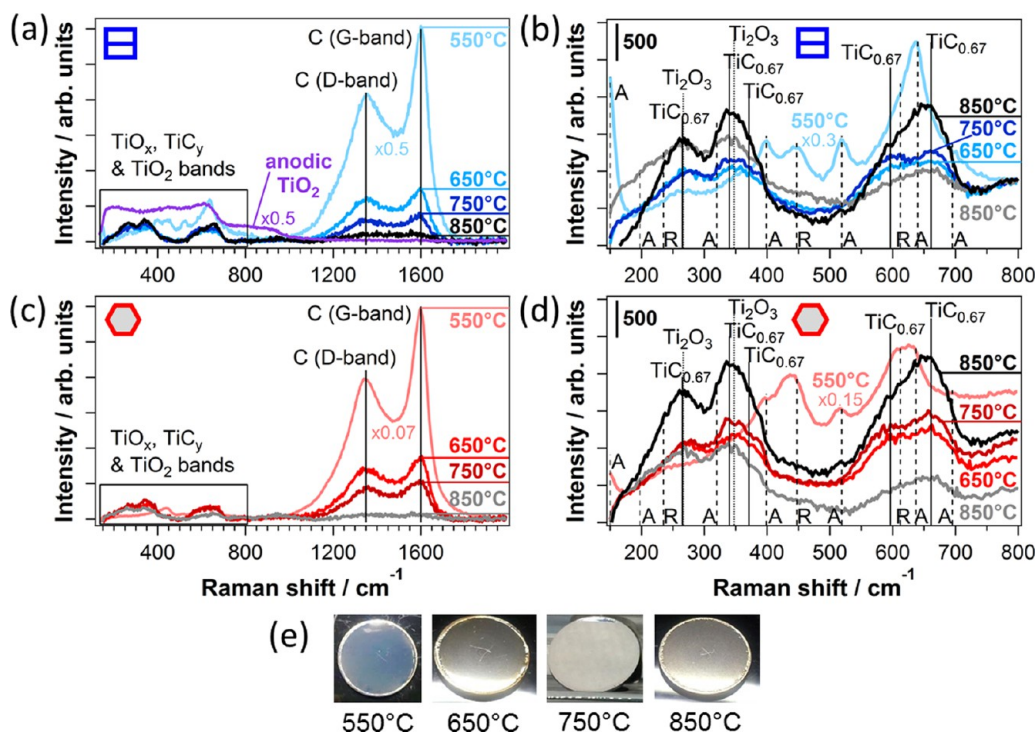


Figure 4. Micro-Raman spectra of TiOC_{550} , TiOC_{650} , and TiOC_{750} on top of (a, b) $\sim\text{Ti}\{10\bar{1}0\}$ and (c, d) $\sim\text{Ti}\{0001\}$ and of two spots on TiOC_{850} with different optical appearances (black and gray spectra). Purple spectrum in (a): as-grown anodic TiO_2 . (b, d) Spectral range marked by the box in (a, c). Baseline correction: (a, c) subtraction of a fourth-order polynomial function; constant shift to a common level at (b) 800 cm^{-1} and (d) 150 cm^{-1} . (e) Photographs of TiOC specimen.

XP spectra of TiOC_{650} (Figure 3b,f) suggest an exceptional surface chemistry on top of substrate grains of type D ($\sim\text{Ti}\{10\bar{1}0\}$; see Table 1): on these grains, the conversion of the anodic film to TiC (TiO) and TiO_x phases is significantly lower and slightly less graphitic carbon is generated on the surface. This is in line with the TiC/ TiO_2 and C/BG chemical maps (Figure 2c), which show a high density of dark spots and thus a lower average content of TiC (TiO) and carbon in the TiOC on top of these grains. The variation in the surface chemistry of TiOC_{650} on top of the other types of substrate grains is less strong. On TiOC_{750} , a pronounced substrate grain-dependent oxide film reduction can be observed, with the highest fraction of TiC (TiO) and TiO_x being present on top of substrate grains D and E, with $50^\circ \leq \Phi \leq 90^\circ$ ($\sim\text{Ti}\{hki0\}$), and the lowest, on substrate grains A and B, with $0^\circ \leq \Phi \leq 40^\circ$ ($\sim\text{Ti}\{0001\}$), which is in accordance with the chemical maps (Figures 3c,g and 2b). At the same time, the total amount of graphitic and carbidic carbon species in TiOC_{750} is slightly higher on substrate grains with $50^\circ \leq \Phi \leq 90^\circ$ ($\sim\text{Ti}\{hki0\}$) than that on substrate grains with $0^\circ \leq \Phi \leq 40^\circ$ ($\sim\text{Ti}\{0001\}$). An intermediate composition is found on substrate grains C, with $40^\circ \leq \Phi \leq 50^\circ$. No difference is visible in the XP spectra of TiOC_{850} on differently oriented substrate grains, which confirms the homogeneous contrast of its chemical maps (Figures 3d,h and 2d). The highest overall fraction of TiC is found in TiOC_{750} on top of $\sim\text{Ti}\{hki0\}$ grains. The highest overall amount of (amorphous or graphitic) carbon is found in TiOC_{650} on top of all substrate grains except for $\sim\text{Ti}\{10\bar{1}0\}$ (Figures 3f and S2). Considering only TiOC_{650} and TiOC_{750} , an almost opposite chemical surface composition is observed on $\sim\text{Ti}\{10\bar{1}0\}$ and $\sim\text{Ti}\{0001\}$ substrate grains: TiOC_{650} contains a high amount of TiC and C on $\sim\text{Ti}\{0001\}$ and a

low amount on $\sim\text{Ti}\{10\bar{1}0\}$, whereas the contrary is found for TiOC_{750} .

The SPEM results reveal that both annealing temperature and substrate texture determine the TiOC surface chemistry. TiC-rich TiOC can be synthesized through carburization of anodic TiO_2 at 650 or 750 °C. However, it depends on substrate texture, whether a higher average TiC content is obtained in TiOC_{650} or in TiOC_{750} under the given annealing conditions (see Figure S1): in the case of a Ti substrate with a large fraction of $\sim\text{Ti}\{hki0\}$ grains, the average TiC content can be expected to be higher in TiOC_{750} than that in TiOC_{650} ; a Ti substrate with grain orientations restricted to $40^\circ \leq \Phi \leq 50^\circ$ yields most likely a similar average TiC content in TiOC_{650} and TiOC_{750} ; finally, a Ti substrate with mainly $\sim\text{Ti}\{0001\}$ grains can be expected to yield a higher average TiC content in TiOC_{650} than that in TiOC_{750} .

Micro-Raman spectroscopy was performed to gain information on the substrate grain-dependent structure and chemical composition of the anodic TiO_2 before and after carbothermal treatment at different temperatures. Figure 4 depicts the Raman spectra of as-anodized TiO_2 and of TiOC_{550} , TiOC_{650} , and TiOC_{750} on top of $\sim\text{Ti}\{10\bar{1}0\}$ and $\sim\text{Ti}\{0001\}$ substrate grains, for which SPEM reveals a clearly different TiOC composition. As the initial grain boundaries of the titanium substrate vanished after carbothermal treatment at 850 °C, Raman spectra of TiOC_{850} were acquired on several spots of different appearance in the optical microscope (black and gray spectra in Figure 4). Photographs of the TiOC surfaces are shown in Figure 4e. An alternative representation of the micro-Raman spectra is given in Figure S3. The peaks at 1350 and 1600 cm^{-1} in Figure 4a,c correspond to the D and G bands of the nanocrystalline graphitic carbon.²³ Figure 4b,d depicts the spectral range of the bands associated with Raman-active TiO_2 ,

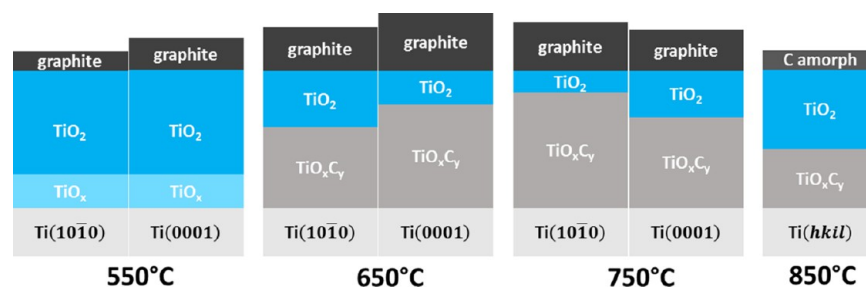


Figure 5. Schematic representation of the cross-sectional composition of TiOC on top of $\sim\text{Ti}(10\bar{1}0)$ and $\sim\text{Ti}(0001)$ substrate grains for the different annealing temperatures. The substrate grain orientations of TiOC_{850} are unknown due to grain growth during the thermal treatment.

TiO_x or TiC_y phases. Anatase and rutile TiO_2 are characterized by vibrational bands marked with dashed lines and are labeled as A and R, respectively.^{24,25} Peaks at ~ 267 and ~ 347 cm^{-1} , marked with dotted lines, can be attributed to the most intense Raman signals of Ti_2O_3 .^{26,27} Stoichiometric TiC has no Raman-active vibrational modes. However, the disorder in the cubic (NaCl) crystal structure of TiC_y (with $y < 1$) that is induced by carbon vacancies activates the A_{1g} , E_g , and T_{2g} modes for Raman scattering.²⁸ The Raman spectrum of $\text{TiC}_{0.67}$ has been reported to contain five peaks at 265, 340, 372, 596, and 661 cm^{-1} ;²⁹ they are labeled in Figure 4b,d.

The absence of distinct bands associated with crystalline (rutile or anatase) TiO_2 evidences that the as-grown anodic film is amorphous (purple spectrum in Figure 4a). Carbothermal treatment at 550 °C leads to crystallization of the oxide, generating a mixed phase of rutile and anatase, and to a slight reduction, which is evidenced by the features ascribed to Ti_2O_3 . The highest fraction of rutile is detected on top of $\sim\text{Ti}(0001)$ (compare Figures 4b,d and S3).^{7,30} There are no bands associated with TiC_y phases in the spectra of TiOC_{550} . The blue optical appearance of TiOC_{550} indicates that the ~ 53 nm thick anodic oxide film is only slightly reduced, where the color is most likely a result of interference effects in combination with color centers, for example, due to oxygen vacancies (Figure 4e). Note that the as-grown anodic film has a different blue color, which arises from interference effects only (see the Supporting Information of ref 7).

No graphitic carbon is detected prior to the carbothermal treatment. The carbon bands are intense for TiOC_{550} and continuously decrease with increasing annealing temperature on both types of substrate grains (Figure 4a,c). The Raman signal of the graphitic carbon is notably enhanced for TiOC_{550} compared to that observed for TiOC_{650} and TiOC_{750} , whereas the XP spectra suggest that there is less elemental carbon on TiOC_{550} (Figure 3). This enhancement of the carbon bands can be explained by resonant Raman scattering with the π -states of graphite, which is typical for thin graphite layers with a low content of defects.³¹ The optically transparent anodic oxide underneath the graphite layer may contribute to this enhancement.³²

The Raman spectra of the TiO_2 , TiO_x , and TiC_y phases considerably change when the annealing temperature is enhanced from 550 to 650 °C (Figures 4b,d and S3). Whereas the anatase and rutile phases of TiO_2 are present in TiOC_{550} , the corresponding bands (in particular, the characteristic low-frequency band of anatase) are not visible in the spectra of TiOC_{650} , TiOC_{750} , and TiOC_{850} . Instead, Raman-active TiO_x and TiC_y phases appear and, at the same time, the optical appearance of TiOC changes to metallic gray (Figure 4e). This indicates that the oxide film is completely converted to a

TiO_xC_y phase, which is mainly a solid solution of TiO and TiC and has been reported to have semi-metallic properties,^{5,14,21,33} through carbothermal treatments at 650, 750, and 850 °C. The fraction of TiO_2 on the surface, detected with SPEM, appears to be too small to considerably contribute to the Raman response. Only the slightly enhanced signal intensity at 447 cm^{-1} (E_g band of rutile TiO_2) in the gray spectrum of TiOC_{850} with respect to that in the black spectrum may be related to the presence of TiO_2 (Figures 4b and S3). Without data on well-defined TiO_xC_y reference materials, it is not possible to quantify the phase composition and stoichiometry of the TiO_xC_y phase in the bulk of TiOC using Raman spectroscopy. Therefore, the observed differences between the Raman responses of TiOC_{650} , TiOC_{750} , and TiOC_{850} can only be interpreted in a qualitative manner and suggest an effect of the annealing temperature on the stoichiometry and/or defectivity of the converted films.^{28,29} In the case of TiOC_{650} and TiOC_{750} , a weak substrate grain orientation effect on the Raman response can also be observed (see Figure S3). A relation of the properties of TiOC_{850} with the initial substrate grains is not possible, but local variations in phase composition are evidenced by notable differences between the black and gray spectra in Figure 4b,d (see also Figure S3).

A thorough investigation of TiO_{550} with micro-Raman spectroscopy is reported in ref 7, in which a marked relation between the substrate grain orientations and crystalline phases of TiO_2 as well as the amount of deposited graphitic carbon was found.

3. DISCUSSION

The presented results show that the final physicochemical properties of carbothermally produced TiOC on Ti_{poly} , such as the chemical composition, phase composition, and surface morphology, depend on the annealing temperature and underlying substrate grain orientations. It should be noted that the gas atmosphere during the carbothermal treatment constitutes an important synthesis parameter as well: very similar chemical maps to those of TiOC_{750} are obtained by carburization of planar anodic TiO_2 films on Ti_{poly} under ultrahigh vacuum conditions using ethylene as a carbon source.⁵

To summarize the results obtained with SPEM and micro-Raman spectroscopy, Figure 5 depicts simplified schematic models representing the cross-sectional compositions of TiOC on top of substrate grains with $\sim\text{Ti}(10\bar{1}0)$ and $\sim\text{Ti}(0001)$ orientations for the different annealing temperatures. TiO_xC_y represents here the solid solution of TiC and TiO, as well as TiO_x phases. The different thicknesses of the compact, as-grown anodic TiO_2 on top of differently oriented substrate grains, which have been reported in the literature,^{34–36} are neglected in the depicted models. The film thickness is

assumed to remain constant for all carbothermal treatments. Compositional gradients are simplified to defined phase boundaries. Carburization at 650 and 750 °C is found to generate TiOC films with an inhomogeneous surface chemistry on individual grains: in the case of TiOC₆₅₀, SPEM reveals micrometer-sized spots on $\sim\text{Ti}(10\bar{1}0)$, with compositions that differ from the average (Figure 2c), and in the case of TiOC₇₅₀, a different chemical composition is observed at grain boundaries (Figure 2b). Furthermore, on the nanometric scale, a patched surface composition of TiOC, with carbon, TiO₂, and TiO_xC_y (if present) side by side, is possible.⁵ For the sake of simplicity, only the grain area-averaged chemical composition is considered in Figure 5. This gives rise to the layered film structure of the models, which is in line with previously performed angle-resolved XPS measurements on TiO_xC_y-rich TiOC⁵ and is supported by the present results of XP and micro-Raman spectroscopies, which reveal that the TiO_xC_y phase in TiOC₈₅₀ is covered by a TiO₂ film of at least ~ 1.4 nm (estimated from the photoelectron escape depth in TiO₂).

Carbothermal treatment at 550 °C yields a C/TiO₂ composite, with TiO_x species in the oxide film and a substrate grain-dependent amount of graphitic carbon on the surface, which is higher on top of $\sim\text{Ti}(0001)$ than that on top of $\sim\text{Ti}\{10\bar{1}0\}$, as reported in ref 7. At 650, 750, and 850 °C, the anodic TiO₂ film is converted to TiO_xC_y in the bulk, as suggested by the Raman results (Figure 4), but contains temperature- and substrate grain-dependent fractions of TiO₂ and carbon at the surface, as seen with SPEM (Figures 2 and 3). The carbon is mainly graphitic (denoted by graphite) on TiOC₅₅₀, TiOC₆₅₀, and TiOC₇₅₀ and amorphous (denoted by C amorph) on TiOC₈₅₀. In the case of TiOC₆₅₀, there is more TiO₂ and less carbon on $\sim\text{Ti}(10\bar{1}0)$ than those on $\sim\text{Ti}(0001)$. In the case of TiOC₇₅₀, there is less TiO₂ and more carbon on $\sim\text{Ti}(10\bar{1}0)$ than those on $\sim\text{Ti}(0001)$. The fractions of TiO₂ and carbon in TiOC₆₅₀ on $\sim\text{Ti}(10\bar{1}0)$ are similar to the respective fractions in TiOC₇₅₀ on $\sim\text{Ti}(0001)$, but there is more TiO₂ and C in TiOC₆₅₀ on $\sim\text{Ti}(0001)$ than those in TiOC₇₅₀ on $\sim\text{Ti}(10\bar{1}0)$. After carburization at 850 °C, the amount of carbon is significantly lower and the amount of TiO₂ is significantly higher than those after carburization at 750 and 650 °C.

The physicochemical properties of TiOC can be understood as resulting from several parallel processes during and after carburization that are affected by temperature and substrate texture, which will be discussed in the following.

3.1. Crystallization of TiO₂ and Reactive Decomposition of C₂H₂. During carbothermal treatments at high temperatures, the amorphous anodic TiO₂ crystallizes to anatase and/or rutile phases before C₂H₂ is added to the process. The crystallization kinetics depends on the temperature and orientation of the Ti substrate, which has consequences for the reaction of the surface with C₂H₂.⁷ Because of the higher activity of anatase TiO₂ compared to that of amorphous TiO₂ toward the reactive decomposition of C₂H₂, the substrate grain-dependent crystallization results in a substrate grain-dependent amount of graphitic carbon on the surface of TiOC₅₅₀.⁷ Also, at higher temperatures, the substrate texture may affect the crystallization of anodic TiO₂ and thus the reactive decomposition of C₂H₂. In particular, the peculiar properties of TiOC₆₅₀ on top of $\sim\text{Ti}\{10\bar{1}0\}$, namely, the presence of spots with a lower carbon coverage and a lower fraction of TiC compared to the average, may be ascribed to the

formation of a polycrystalline TiO₂ film on these grains, exposing facets of very different reactivities. Furthermore, the significantly lower amount of carbon on TiOC₈₅₀ could be related to a low reactivity of the, most likely rutile-rich, TiO₂ film that forms at 850 °C prior to the addition of C₂H₂.³⁷ Besides the reactivity of the surface, the sticking coefficient of C₂H₂ on TiO₂ and the desorption probability of possible reaction intermediates, both of which depend on temperature and surface structure, can play a role in the substrate grain-dependent decomposition efficiency. Because of the concomitant diffusion of carbon into the bulk and generation of TiC at temperatures of 650 °C and higher, the final carbon content at the surface is not determined only by carbon layer formation.

3.2. Conversion of TiO₂ to TiC and Material Transport in TiO₂ and Ti. To explain the observed temperature-dependent average chemical composition of TiOC, thermodynamic considerations need to be taken into account. First, sufficiently high temperatures are required to convert TiO₂ into a solid solution of TiC and TiO.⁵ Second, the final bulk composition is mostly determined by thermally activated diffusion of both carbon into the compact anodic TiO₂ and oxygen and carbon into the Ti substrate.¹⁴ The average amount of carbon on the surface decreases from 650 to 850 °C, which can be attributed partly to the higher diffusion kinetics of carbon at higher temperatures and partly to the lower carbon-formation efficiency. It is noteworthy that the amorphous carbon found on TiOC₈₅₀ most likely originates from contamination of TiO₂ that is not covered by graphitic carbon from the thermal C₂H₂ treatment, after exposure to ambient air. The results obtained with micro-Raman spectroscopy suggest a temperature- and substrate grain-dependent stoichiometry and/or defectivity of the TiO_xC_y phase in TiOC, which is very likely a consequence of the temperature- and substrate grain-dependent carbon supply and diffusion kinetics. At 850 °C, both oxygen and, in particular, carbon can diffuse into the Ti substrate, promoting the formation of a carbon-poor TiO_xC_y phase.¹⁴

The main influence of substrate grain orientations on the conversion may be an indirect effect controlled by the initial formation of polycrystalline TiO₂, with a substrate grain-dependent phase composition and preferential orientation. First-principles calculations suggest anisotropic migration of carbon in the tetragonal lattices of anatase ($c/a = 2.51$) and rutile TiO₂ ($c/a = 0.64$).^{38,39} Therefore, substrate grain-dependent material transport in TiO₂, which brings about substrate texture-dependent conversion time scales of the anodic TiO₂ at a given temperature, may be responsible for the substrate grain-dependent chemical compositions of TiOC₆₅₀ and TiOC₇₅₀. When oxygen and carbon start to diffuse into the Ti substrate, the grain-dependent orientation of the hexagonal Ti lattice ($c/a = 1.58$) is likely to determine the diffusion kinetics^{40,41} and therewith not only the fractions of C and O that remain in the TiO_xC_y phase adjacent to the Ti substrate but also the thickness of the TiO_xC_y layer. In addition, the substrate grain boundaries can affect the conversion of the anodic TiO₂. From the chemical maps of TiOC₇₅₀ (Figure 2b), a different conversion behavior of the anodic film at the boundaries compared to that in the area within the substrate grains can be inferred, suggesting a lower reactivity and/or faster carbon diffusion at the substrate grain boundaries. At 850 °C, substrate grain growth becomes important as well, generating fresh grain boundaries in the oxide film, which can facilitate diffusion of carbon into the bulk.

3.3. Surface Re-Oxidation of TiO_xC_y . Besides the temperature- and grain-dependent conversion of TiO_2 to TiO_xC_y , the final composition of TiOC is affected by the subsequent re-oxidation of the TiC , TiO , and TiO_x species near the surface to TiO_2 and graphitic carbon, due to their relative thermodynamic instability at room temperature and in the presence of oxygen.⁵ Re-oxidation was reported to happen during exposure of TiO_xC_y -rich films to ambient air and even during cooling down in reducing atmosphere at the end of a carbothermal treatment, when the temperature dropped below a certain threshold value.⁵ As the intrinsic inertness toward re-oxidation depends on the chemical composition of TiOC (in particular, on the stoichiometry of the TiO_xC_y phase),⁵ a substrate grain effect on the re-oxidation rate can be expected for TiOC_{650} and TiOC_{750} . In the case of TiOC_{850} , for which local variations in chemical composition that cannot be related to initial substrate grain orientations are observed, the intrinsic inertness is likely to vary accordingly on areas of different compositions. A high amount of graphitic carbon on the surface of TiOC after carburization could retard the re-oxidation process, as carbon doping or carbon coating of TiO_2 is known to suppress the crystalline phase transformations of TiO_2 and reduce TiO_2 crystallite growth,^{42,43} both of which are processes that require atomic re-organization, as does re-oxidation. This provides a possible explanation for the observation that there is less TiO_2 on TiOC_{650} and TiOC_{750} than that on TiOC_{850} . Furthermore, the inverse trend of carbon and TiO_2 at the surfaces of TiOC_{650} and TiOC_{750} on top of $\sim\text{Ti}(0001)$ and $\sim\text{Ti}\{10\bar{1}0\}$ may be partially ascribed to the possible retardation of TiO_xC_y re-oxidation on those substrate grains on which TiOC contains a high fraction of carbon. Therefore, not only the TiO_2 conversion time scale but also the TiOC re-oxidation time scale is effectively determined by the substrate texture. Independent of the substrate texture, the surface oxide of TiOC_{550} is almost stoichiometric within the depth that can be analyzed with SPEM so that no substrate grain-dependent intrinsic stability can be deduced here. It is noteworthy that the substrate grain-dependent fraction of TiO_2 observed with SPEM on TiOC_{550} is a consequence of the substrate grain-dependent thickness of the carbon layer, which attenuates photoelectrons from the covered TiO_2 .⁷

4. CONCLUSIONS

The presented results on the annealing temperature and substrate grain-dependent conversion of compact anodic TiO_2 on Ti_{poly} to TiOC reveal that both annealing temperature and substrate texture majorly influence this process. By means of a spectromicroscopic multimodal approach, employing EBSD, SEM, SPEM, and micro-Raman spectroscopy, it was found that the anodic films on top of differently oriented substrate grains have individual conversion and re-oxidation time scales. A combination of temperature- and substrate grain-dependent processes, such as crystallization, reactive carbon deposition, conversion to TiO_xC_y , and re-oxidation of the surface, plays a major role in the definition of the heterogeneous physicochemical properties of TiOC films. A deep understanding of such an interplay constitutes an essential point toward the development of novel transition metal oxycarbide-based synergistic supports for use in (electro)catalytic systems with improved performance. On the basis of the present findings, the spatially selective degradation of $\text{Pt}/\text{TiOC}_{750}/\text{Ti}_{\text{poly}}$ during ethanol electro-oxidation¹⁵ can be ascribed to the substrate grain-dependent chemical composition of TiOC_{750} , which determines the overall

chemical stability of the catalytic system in concentrated phosphoric acid at elevated temperatures.

5. EXPERIMENTAL SECTION

5.1. Sample Preparation. Disks of 1 mm thickness and 10–15 mm diameter were cut from a 20 mm diameter Ti_{poly} rod (99.6% purity, temper annealed; Advent Ltd., England). One side of the disks was mechanically and electrochemically polished, following the procedure described in refs 7 and 14. The areas of investigation were marked with a cross-scratch on the samples using a tungsten needle. The electropolished Ti disks were thoroughly cleaned in an ultrasonic bath with ethanol (technical grade), isopropanol (high purity), and deionized (DI) water (Millipore-Milli-Q system, 18.2 M Ω).

Compact amorphous, ~ 53 nm thick TiO_2 films were produced by potentiostatic electrochemical anodization in a home-built Teflon electrochemical cell with a two-electrode configuration using a DC power supply controlled by a multimeter. Anodization was carried out at 20 V for 600 s in 0.1 M sulfuric acid (H_2SO_4 , suprapure, 96%; Merck, Germany) electrolyte at room temperature with a platinum mesh counter electrode.¹⁴ The anodic films were rinsed with DI water and dried in an argon (Ar 4.8; Linde, Germany) stream.

Carbothermal treatment was conducted in a tubular quartz reactor under controlled gas flow. For carburization, the following procedure was applied: (i) purging for 2 h with a high flow of Ar to remove air, (ii) heating at a constant rate to $T = 550, 650, 750,$ or 850 °C in 200 standard cubic centimeters per minute (sccm) Ar, (iii) dwelling for 60 min at T , (iv) addition of 0.5 flow % of acetylene (C_2H_2 , solvent-free; Linde, Germany) for 5 min, (v) dwelling for 60 min at T in Ar, (vi) cooling to room temperature. The carburized anodic films are termed TiOC_T throughout the text, where T represents the annealing temperatures 550, 650, 750, and 850 °C.

5.2. EBSD and SEM. The crystallographic orientation of the electropolished Ti substrate was mapped by EBSD using a FEI XL30 scanning electron microscope operated at a 20 kV accelerating voltage and equipped with a TSL-EDAX EBSD system. The step size of the EBSD map was set to 2 μm , which led to a suitable spatial resolution of the microstructure. The surface morphology of carburized TiO_2 was investigated with a field-emission SEM based on a Gemini column in a Zeiss CrossBeam NVision 40 system. Micrographs were taken with the in-lens secondary electron detector, using an acceleration voltage of 4 kV and working distances of 4–7 mm.

5.3. Micro-Raman Spectroscopy. Micro-Raman spectroscopy was used to investigate the crystalline phase composition of the carbothermally treated films. A dispersive Renishaw Raman Microscope (Type 1000) equipped with a CCD detector, a Leica DM LM microscope, and a multiline argon-ion gas laser (Stellar-Pro Select 150 of MODU-Laser) set at 514 nm were used to analyze the chemistry and structure of the films. The laser was unpolarized, the size of the focused laser spot on the sample was about 5 μm (using the 50 \times magnification of the optical microscope), and the excitation energy of the laser was set to ≤ 20 mW, which was low enough to avoid chemical modifications or sample damage during the selected exposure times. Backscattered Raman signals were recorded with a resolution of about 1 cm^{-1} from 2000 to 146 cm^{-1} (lower wavenumbers were cut off by the notch filter), with an acquisition time of 1×50 s, and from 800 to 146 cm^{-1} , with an acquisition time of 2×100 s. For baseline correction (background fluorescence), a fourth-order polynomial function

was subtracted from the raw data of the extended spectra and the small-range spectra were only shifted to a common background level.

5.4. SPEM. SPEM was performed at the ESCA microscopy beamline at the Elettra Synchrotron Facility in Trieste, where the X-ray photon beam was demagnified by a Zone Plate to a submicron spot of about 150 nm onto the sample, which was then rastered to produce an image by detecting the photoelectrons generated from the sample.⁴⁴ In this work, the photon energy was set to 756 eV. The incident X-ray beam was normal to the sample surface, whereas angle θ between the hemispherical electron analyzer (HEA) and the sample surface was 30°, providing high surface sensitivity. Photoelectron maps of 50 × 50 μm^2 were recorded by sampling the surface with a step of 0.2 μm and a dwell time of 60 ms per pixel. The HEA was equipped with a multichannel electron detector, which simultaneously acquires 48 maps (channels), each tuned at a specific photoelectron energy within a selected energy window. This allowed to (i) extract XP spectra from selected areas of the acquired photoelectron micrograph, with an energy window of 7.8 eV and a step of 0.164 eV and (ii) to remove the topographic contributions to the photoelectron micrographs and extract the chemical contrast. The chemical contrast micrographs (chemical maps) were obtained by choosing two sets of maps from the recorded 48 maps that were acquired either in the energy range of a photoelectron peak or in the energy range of the background signal, integrating them to obtain two effective maps corresponding to the photoelectron signal in the two spectral ranges and obtaining their ratio.⁴⁵ In that way, peak over background (C/BG, TiO₂/BG) or peak A over peak B (TiC/TiO₂, TiO_x/TiO₂) chemical maps were obtained from the photoelectron maps acquired in the spectral regions of the C 1s and Ti 2p_{3/2} core levels.

■ ASSOCIATED CONTENT

● Supporting Information

The Supporting Information is available free of charge on the ACS Publications website at DOI: 10.1021/acsomega.6b00472.

Alternative representation of the XP spectra; alternative representation of the micro-Raman spectra (PDF)

■ AUTHOR INFORMATION

Corresponding Authors

*E-mail: celine.ruediger@tum.de (C.R.).

*E-mail: Julia.Kunze@uibk.ac.at. Tel: +43 (0) 512 507 58013 (J.K.-L.).

ORCID

Celine Rüdiger: 0000-0003-4396-7011

Stefano Agnoli: 0000-0001-5204-5460

Gaetano Granozzi: 0000-0002-9509-6142

Present Addresses

[∇]Helmholtz-Zentrum Berlin (HZB), Institute for Solar Fuels, Hahn-Meitner-Platz 1, 14109 Berlin, Germany (M.F.).

[○]Advanced Light Source (ALS) and Joint Center for Energy Storage Research (JCESR), Lawrence Berkeley National Laboratory, 1 Cyclotron Road, Berkeley, CA 94720, United States (C.V.-V.).

[◆]Shell Global Solutions International B.V., P.O. Box 38000, 1030 BN Amsterdam, The Netherlands (J.H.).

Funding

This research was mainly supported by funds of the EU RTD Framework Program FP7 (FP7-NMP-2012-SMALL-6, project title DECORE, project number 309741). Marco Favaro obtained financial support from Fondazione Cariparo.

Notes

The authors declare no competing financial interest.

■ ACKNOWLEDGMENTS

The authors thank the EU RTD Framework Program FP7 (FP7-NMP-2012-SMALL-6, project title DECORE, project number 309741) for financial support. Marco Favaro acknowledges Fondazione Cariparo for financial support. Furthermore, the chair of Technical Chemistry II at the Technische Universität München (TUM) is acknowledged for the permission to conduct Raman studies. The authors are especially grateful to Prof. Andreas Jentys for his assistance during the Raman spectroscopy measurements.

■ ABBREVIATIONS

SEM, scanning electron microscopy; SPEM, scanning photoelectron microscopy; EBSD, electron backscatter diffraction; XP, X-ray photoelectron

■ REFERENCES

- (1) Henderson, M. A. Structural Sensitivity in the Dissociation of Water on TiO₂ Single-Crystal Surfaces. *Langmuir* **1996**, *12*, 5093–5098.
- (2) Koper, M. T. M. Structure Sensitivity and Nanoscale Effects in Electrocatalysis. *Nanoscale* **2011**, *3*, 2054–2073.
- (3) Bandarenka, A. S.; Koper, M. T. M. Structural and Electronic Effects in Heterogeneous Electrocatalysis: Toward a Rational Design of Electrocatalysts. *J. Catal.* **2013**, *308*, 11–24.
- (4) Yoon, T. H. Applications of Soft X-Ray Spectromicroscopy in Material and Environmental Sciences. *Appl. Spectrosc. Rev.* **2009**, *44*, 91–122.
- (5) Calvillo, L.; Fittipaldi, D.; Rüdiger, C.; Agnoli, S.; Favaro, M.; Valero-Vidal, C.; Di Valentin, C.; Vittadini, A.; Bozzolo, N.; Jacomet, S.; Gregoratti, L.; Kunze-Liebhäuser, J.; Pacchioni, G.; Granozzi, G. Carbothermal Transformation of TiO₂ into TiO_xC_y in UHV: Tracking Intrinsic Chemical Stabilities. *J. Phys. Chem. C* **2014**, *118*, 22601–22610.
- (6) Calvillo, L.; Valero-Vidal, C.; Agnoli, S.; Sezen, H.; Rüdiger, C.; Kunze-Liebhäuser, J.; Granozzi, G. Combined Photoemission Spectroscopy and Electrochemical Study of a Mixture of (Oxy)carbides as Potential Innovative Supports and Electrocatalysts. *ACS Appl. Mater. Interfaces* **2016**, *8*, 19418–19427.
- (7) Rüdiger, C.; Favaro, M.; Valero-Vidal, C.; Calvillo, L.; Bozzolo, N.; Jacomet, S.; Hejny, C.; Gregoratti, L.; Amati, M.; Agnoli, S.; Granozzi, G.; Kunze-Liebhäuser, J. Fabrication of Ti Substrate Grain Dependent C/TiO₂ Composites through Carbothermal Treatment of Anodic TiO₂. *Phys. Chem. Chem. Phys.* **2016**, *18*, 9220–9231.
- (8) Ignaszak, A.; Song, C.; Zhu, W.; Zhang, J.; Bauer, A.; Baker, R.; Neburchilov, V.; Ye, S.; Campbell, S. Titanium Carbide and Its Core-Shell Derivative TiC@TiO₂ as Catalyst Supports for Proton Exchange Membrane Fuel Cells. *Electrochim. Acta* **2012**, *69*, 397–405.
- (9) Kim, D.-Y.; Han, S.-B.; Lee, Y.-W.; Park, K.-W. Core-Shell Nanostructure Supported Pt Catalyst with Improved Electrocatalytic Stability in Oxygen Reduction Reaction. *Mater. Chem. Phys.* **2013**, *137*, 704–708.
- (10) Zana, A.; Rüdiger, C.; Kunze-Liebhäuser, J.; Granozzi, G.; Reeler, N. E. A.; Vosch, T.; Kirkensgaard, J. J. K.; Arenz, M. Core-Shell TiO₂@C: Towards Alternative Supports as Replacement for High Surface Area Carbon for PEMFC Catalysts. *Electrochim. Acta* **2014**, *139*, 21–28.

- (11) Xiong, L.; Manthiram, A. Synthesis and Characterization of Methanol Tolerant Pt/TiO_x/C Nanocomposites for Oxygen Reduction in Direct Methanol Fuel Cells. *Electrochim. Acta* **2004**, *49*, 4163–4170.
- (12) Liu, Y.; Kelly, T. G.; Chen, J. G.; Mustain, W. E. Metal Carbides as Alternative Electrocatalyst Supports. *ACS Catal.* **2013**, *3*, 1184–1194.
- (13) Roca-Ayats, M.; Garcia, G.; Pena, M. A.; Martinez-Huerta, M. V. Titanium Carbide and Carbonitride Electrocatalyst Supports: Modifying Pt-Ti Interface Properties by Electrochemical Potential Cycling. *J. Mater. Chem. A* **2014**, *2*, 18786–18790.
- (14) Rüdiger, C.; Maglia, F.; Leonardi, S.; Sachsenhauser, M.; Sharp, I. D.; Paschos, O.; Kunze, J. Surface Analytical Study of Carbothermally Reduced Titania Films for Electrocatalysis Application. *Electrochim. Acta* **2012**, *71*, 1–9.
- (15) Rüdiger, C.; Brumbarov, J.; Wiesinger, F.; Leonardi, S.; Paschos, O.; Valero Vidal, C.; Kunze-Liebhäuser, J. Ethanol Oxidation on TiO_xC_y-Supported Pt Nanoparticles. *ChemCatChem* **2013**, *5*, 3219–3223.
- (16) Calvillo, L.; García, G.; Paduano, A.; Guillen-Villafuerte, O.; Valero-Vidal, C.; Vittadini, A.; Bellini, M.; Lavacchi, A.; Agnoli, S.; Martucci, A.; Kunze-Liebhäuser, J.; Pastor, E.; Granozzi, G. Electrochemical Behavior of TiO_xC_y as Catalyst Support for Direct Ethanol Fuel Cells at Intermediate Temperature: From Planar Systems to Powders. *ACS Appl. Mater. Interfaces* **2016**, *8*, 716–725.
- (17) König, U.; Davepon, B. Microstructure of Polycrystalline Ti and Its Microelectrochemical Properties by Means of Electron-Backscattering Diffraction (EBSD). *Electrochim. Acta* **2001**, *47*, 149–160.
- (18) Okazaki, K.; Conrad, H. Recrystallization and Grain Growth in Titanium: I. Characterization of the Structure. *Metall. Trans.* **1972**, *3*, 2411–2421.
- (19) Murray, J. L.; Wriedt, H. A. Ti-O Phase Diagram. In *Materials Properties Handbook: Titanium Alloys*; Boyer, R., Welsch, G., Collings, E. W., Eds.; ASM International: OH, 1994; p 130.
- (20) Ramqvist, L.; Hamrin, K.; Johansson, G.; Fahlman, A.; Nordling, C. Charge Transfer in Transition Metal Carbides and Related Compounds Studied by ESCA. *J. Phys. Chem. Solids* **1969**, *30*, 1835–1847.
- (21) Favaro, M.; Leonardi, S.; Valero-Vidal, C.; Nappini, S.; Hanzlik, M.; Agnoli, S.; Kunze-Liebhäuser, J.; Granozzi, G. In-Situ Carbon Doping of TiO₂ Nanotubes via Anodization in Graphene Oxide Quantum Dot Containing Electrolyte and Carburization to TiO_xC_y Nanotubes. *Adv. Mater. Interfaces* **2015**, *2*, 1400462–1400472.
- (22) Chu, P. K.; Li, L. Characterization of Amorphous and Nanocrystalline Carbon Films. *Mater. Chem. Phys.* **2006**, *96*, 253–277.
- (23) Ferrari, A. C.; Robertson, J. Interpretation of Raman Spectra of Disordered and Amorphous Carbon. *Phys. Rev. B* **2000**, *61*, 14095–14107.
- (24) Ohsaka, T.; Izumi, F.; Fujiki, Y. Raman Spectrum of Anatase, TiO₂. *J. Raman Spectrosc.* **1978**, *7*, 321–324.
- (25) Porto, S. P. S.; Fleury, P. A.; Damen, T. C. Raman Spectra of TiO₂, MgF₂, ZnF₂, FeF₂, and MnF₂. *Phys. Rev.* **1967**, *154*, 522–526.
- (26) Mooradian, A.; Raccach, P. M. Raman Study of the Semiconductor-Metal Transition in Ti₂O₃. *Phys. Rev. B* **1971**, *3*, 4253–4256.
- (27) Hsu, S.-W.; Yang, T.-S.; Chen, T.-K.; Wong, M.-S. Ion-Assisted Electron-Beam Evaporation of Carbon-Doped Titanium Oxide Films as Visible-Light Photocatalyst. *Thin Solid Films* **2007**, *515*, 3521–3526.
- (28) Klein, M. V.; Holy, J. A.; Williams, W. S. Raman Scattering Induced by Carbon Vacancies in TiC_x. *Phys. Rev. B* **1978**, *17*, 1546–1556.
- (29) Amer, M.; Barsoum, M. W.; El-Raghy, T.; Weiss, I.; Leclair, S.; Liptak, D. The Raman Spectrum of Ti₃SiC₂. *J. Appl. Phys.* **1998**, *84*, 5817–5819.
- (30) Zhang, J.; Li, M.; Feng, Z.; Chen, J.; Li, C. UV Raman Spectroscopic Study on TiO₂. I. Phase Transformation at the Surface and in the Bulk. *J. Phys. Chem. B* **2006**, *110*, 927–935.
- (31) Ferrari, A. C. Raman Spectroscopy of Graphene and Graphite: Disorder, Electron-Phonon Coupling, Doping and Nonadiabatic Effects. *Solid State Commun.* **2007**, *143*, 47–57.
- (32) Wang, Y. Y.; Ni, Z. H.; Shen, Z. X.; Wang, H. M.; Wu, Y. H. Interference Enhancement of Raman Signal of Graphene. *Appl. Phys. Lett.* **2008**, *92*, No. 043121.
- (33) Hahn, R.; Schmidt-Stein, F.; Salonen, J.; Thiemann, S.; Song, Y.; Kunze, J.; Lehto, V.-P.; Schmuki, P. Semimetallic TiO₂ Nanotubes. *Angew. Chem., Int. Ed.* **2009**, *48*, 7236–7239.
- (34) Diamanti, M. V.; Pedferri, M. P.; Schuh, C. A. Thickness of Anodic Titanium Oxides as a Function of Crystallographic Orientation of the Substrate. *Metall. Mater. Trans. A* **2008**, *39*, 2143–2147.
- (35) Davepon, B.; Schultze, J. W.; König, U.; Rosenkranz, C. Crystallographic Orientation of Single Grains of Polycrystalline Titanium and Their Influence on Electrochemical Processes. *Surf. Coat. Technol.* **2003**, *169–170*, 85–90.
- (36) Kudelka, S.; Michaelis, A.; Schultze, J. W. Effect of Texture and Formation Rate on Ionic and Electronic Properties of Passive Layers on Ti Single Crystals. *Electrochim. Acta* **1996**, *41*, 863–870.
- (37) Biedrzycki, J. J.; Livraghi, S.; Corazzari, I.; Mino, L.; Spoto, G.; Giamello, E. On the Redox Mechanism Operating along C₂H₂ Self-Assembly at the Surface of TiO₂. *Langmuir* **2015**, *31*, 569–577.
- (38) Tsetseris, L. Stability and Dynamics of Carbon and Nitrogen Dopants in Anatase TiO₂: A Density Functional Theory Study. *Phys. Rev. B* **2010**, *81*, No. 165205.
- (39) Tsetseris, L. Configurations, Electronic Properties, and Diffusion of Carbon and Nitrogen Dopants in Rutile TiO₂: A Density Functional Theory Study. *Phys. Rev. B* **2011**, *84*, No. 165201.
- (40) Quinn, C. J.; Kohlstedt, D. L. Solid-State Reaction Between Titanium Carbide and Titanium Metal. *J. Am. Ceram. Soc.* **1984**, *67*, 305–310.
- (41) Vykhodets, V. B.; Kurennykh, T. E.; Fishman, A. Y. Identification of Heterogeneous State and Trajectories of Interstitials in the Titanium-Oxygen System Using Precise Diffusion Experiment. *Defect Diffus. Forum* **1997**, *143–147*, 79–84.
- (42) Tsumura, T.; Kojitani, N.; Izumi, I.; Iwashita, N.; Toyoda, M.; Inagaki, M. Carbon Coating of Anatase-Type TiO₂ and Photoactivity. *J. Mater. Chem.* **2002**, *12*, 1391–1396.
- (43) Enache, C. S.; Schoonman, J.; van de Krol, R. Addition of Carbon to Anatase TiO₂ by N-Hexane Treatment – surface or Bulk Doping? *Appl. Surf. Sci.* **2006**, *252*, 6342–6347.
- (44) Abyaneh, M. K.; Gregoratti, L.; Amati, M.; Dalmiglio, M.; Kiskinova, M. Scanning Photoelectron Microscopy: A Powerful Technique for Probing Micro and Nano-Structures. *e-J. Surf. Sci. Nanotechnol.* **2011**, *9*, 158–162.
- (45) Gregoratti, L.; Barinov, A.; Benfatto, E.; Cautero, G.; Fava, C.; Lacovig, P.; Lonza, D.; Kiskinova, M.; Tommasini, R.; Mähl, S.; Heichler, W. 48-Channel Electron Detector for Photoemission Spectroscopy and Microscopy. *Rev. Sci. Instrum.* **2004**, *75*, 64–68.